Chaos, Solitons and Fractals 88 (2016) 126–142

Contents lists available at ScienceDirect

Chaos, Solitons and Fractals

Nonlinear Science, and Nonequilibrium and Complex Phenomena

journal homepage: www.elsevier.com/locate/chaos

Dynamic bifurcations on financial markets

M. Kozłowska[a], M. Denys[a], M. Wiliński[a], G. Link[a], T. Gubiec[a], T.R. Werner[a], R. Kutner[a], Z.R. Struzik[b,c,d,*]

[a] Faculty of Physics, University of Warsaw, Pastera 5, 02–093 Warsaw, Poland
[b] The University of Tokyo, 7-3-1 Hongo, Bunkyo-ku, Tokyo 113-0033, Japan
[c] RIKEN Brain Science Institute, 2-1 Hirosawa, Wako-shi 351-0198, Japan
[d] Institute of Theoretical Physics and Astrophysics, The University of Gdańsk, Wita Stwosza 57, 80–952 Gdańsk, Poland

ARTICLE INFO

Article history:
Received 12 November 2015
Revised 10 February 2016
Accepted 2 March 2016
Available online 24 March 2016

PACS:
89.65.Gh
02.50.Ey
02.50.Ga
05.40.Fb
02.30.Mv

Keywords:
Catastrophic bifurcation breakdown
Flickering phenomena
Catastrophic slowing down
Early-warning signal
Worldwide financial crisis

ABSTRACT

We provide evidence that catastrophic bifurcation breakdowns or transitions, preceded by early warning signs such as flickering phenomena, are present on notoriously unpredictable financial markets. For this we construct robust indicators of catastrophic dynamical slowing down and apply these to identify hallmarks of dynamical catastrophic bifurcation transitions. This is done using daily closing index records for the representative examples of financial markets of small and mid to large capitalisations experiencing a speculative bubble induced by the worldwide financial crisis of 2007-08.

1. Introduction

Discontinuous phase transitions in complex systems together with critical phenomena are topics of canonical importance in statistical thermodynamics [3,11,19,28,47,50]. Much as in liquid gas or magnetic systems, during the evolution of complex systems undergoing such phase transitions, one may observe catastrophic breakdowns preceded by flickering phenomenon. These types of discontinuous or critical dynamics are generic illustrations of how small changes can lead to dramatic consequences. Such regime shifts occur as a sophisticated non-trivial phenomenon caused by a catastrophic bifurcation. This means that a catastrophe or tipping point [5,20,50] exists, at which a sudden shift of the system to a contrasting regime may occur.[1]

Arguably, the effects of the critical and catastrophic slowing down are the most refined indicators of whether a system is approaching a critical point or a tipping point – a

* Corresponding author. Tel.: +81356898066.
E-mail addresses: marz.kozlowska@poczta.onet.pl (M. Kozłowska), Mateusz.Denys@fuw.edu.pl (M. Denys), mwilinski@fuw.edu.pl (M. Wiliński), Grzegorz.Link@gmail.com (G. Link), Tomasz.Gubiec@fuw.edu.pl (T. Gubiec), Tomasz.Werner@fuw.edu.pl (T.R. Werner), Ryszard.Kutner@fuw.edu.pl (R. Kutner), z.r.struzik@p.u-tokyo.ac.jp (Z.R. Struzik).

http://dx.doi.org/10.1016/j.chaos.2016.03.005
0960-0779/

[1] For instance, such sudden shifts (or jump discontinuities) of magnetization plotted versus the magnetic field were already found in critical fields, in our earlier work [27], where we studied the influence of lattice ordering on diffusion properties.

tipping point being a synonym for a catastrophic threshold, located at a catastrophic bifurcation transition [6,8,9,17,34]. The problem of whether early-warning signals in the form of critical or catastrophic slowing down phenomena such as those observed in multiple physical systems [28,47] are present on financial markets was posed by Scheffer et al. [48]. Recently, an original approach was put forward by Haldane and May [18], which models banking networks as a banking ecosystem by analogy with nature's ecosystems. Such an approach can offer a valid insight into the financial sector [22,29]. Indeed, one of the most important attainments of the catastrophe theory in the context of economics appears to be in encompassing the concept of complexity. This viewpoint has already been adopted within various economical sectors [1,4,16,46,57–59].

The classification of crises as bifurcations between a stable regime and a novel regime provides a first step towards indentifying signatures which could be used for prediction ([50] and refs. therein). Hence, the problem of the existence of tipping points in financial markets is a heavily researched area. This is because the discovery of predictability, inevitably leads to its elimination, according to one of the most fundamental financial market paradigms. This paradigm states that as a profit can be made (for instance, from predictability), the financial market gradually annihilates such an arbitrage opportunity. Yet, the complex behaviour of financial markets, together with their evolutionary character, continues to prove that it is inherently difficult to identify predictive markers. This in effect posits that such an arbitrage opportunity is routinely present on financial markets and manifested in emergent collective behaviours.

Recently, the economists Nawrocki and Vaga used nonlinear analysis of time series of returns to describe bifurcations on financial markets [51]. Our approach, presented here, is based on the linear and bilinear analysis of detrended indices of quotations. This is because in our case we describe the linear expansion of the stochastic dynamic equation in the vicinity of an equilibrium state (stable or unstable) of the system. Hence, the two approaches should be understood to be complementary. In either case, the existence of the bifurcation transition is not contrary to the above-mentioned market paradigm because, to make a definite prediction, the specific moment of transition must be known. However, such a moment is uncertain (as it is a random variable).

There is a well-known controversy, which is the prime inspiration for our work, concerning two-state transitions on financial markets. Namely, Plerou et al. [36,37] observed two-phase behaviour on financial markets by using empirical transactions and quotes within the intraday data for the 116 most actively traded US stocks during the two-year period of 1994–1995. By examining the fluctuation of volume imbalance, that is by using some conditional probability distribution of the volume imbalance, they found a change in this distribution from uni- to bimodal. This corresponds with a market shift from an equilibrium to an out-of-equilibrium state, where these two different states were interpreted as distinct phases.

In contradiction, Potters and Bouchaud [38] pointed out that the two-phase behaviour of the above-mentioned conditional distribution is a direct consequence of generic statistical properties of the volume traded, and is not a real two-phase phenomenon. In their work on the trading volume, [33] indicated that the bifurcation phenomenon is an artefact of the distribution of trade sizes, which follows a power-law distribution with an exponent belonging to the Lévy stable domain. Further, very recently, Filimonov and Sornette [13] suggested that the trend switching phenomena in financial markets considered in [39–44,53] has a spurious character. They argued that this character stems from the selection of price peaks, which imposes a condition on the statistics of price change and of trade volumes, skewing their distributions.

Nevertheless, the two-phase phenomenon was again examined in the DAX financial index in [60], using minority games and dynamic herding models. They found that this phenomenon is a significant characteristic of financial dynamics, independent of volatility clustering. Furthermore, Jiang et al. [21] observed the bifurcation phenomenon for the Hang-Seng index as non-universal and requiring specific conditions.

The principal goal of our work is to identify and describe the main empirical facts indicating the existence of possible catastrophic bifurcation transitions (CBT) in stock markets of small and mid to large capitalisations. In this work, we consider the bifurcation phenomenon by utilizing the concept of bistability [55] and focusing our attention on the unconditional or joint properties of the catastrophic bifurcation. We further develop and evaluate a number of principal metrics associated with catastrophic bifurcation transitions. Several of them have been previously posed and considered for financial markets ([2,14,23,30,32,45,49] and refs. therein). In particular, we identify hallmarks of the catastrophic bifurcation transition by verifying relevant fundamental indicators, for WIG,[2] DAX, and DJIA daily speculative bubbles on the Warsaw Stock Exchange, Frankfurter Wertpapierbörse, and New York Stock Exchange. That is, we consider the stock markets' speculative bubbles during the 2007-08 worldwide financial crisis for, respectively, small and mid to large capitalisations (cf. Fig. 1).

We concentrate on the analysis of daily financial market data, as we consider that daily data is the most representative as it contains evidence of both the high and the low-frequency trading. That is, daily closing data has an intermediate character containing information both from the intraday trading and from the less frequent, longer-term interday trading span. In addition, because of the existence of well-known intraday patterns, detrending procedures are better established for the daily data than for the intraday case. Both the bullish and the bearish sides of the peaks considered are detrended using a generalised exponential (or Mittag-Leffler function) decorated by oscillatory behaviour (for details see Appendix A). This is because such a function better fits the peaks considered in this work than the commonly used log-periodic function [10,12,54].

[2] The index WIG (Warszawski Indeks Giełdowy) is the main index of the Warsaw Stock Exchange, which is of a small size.

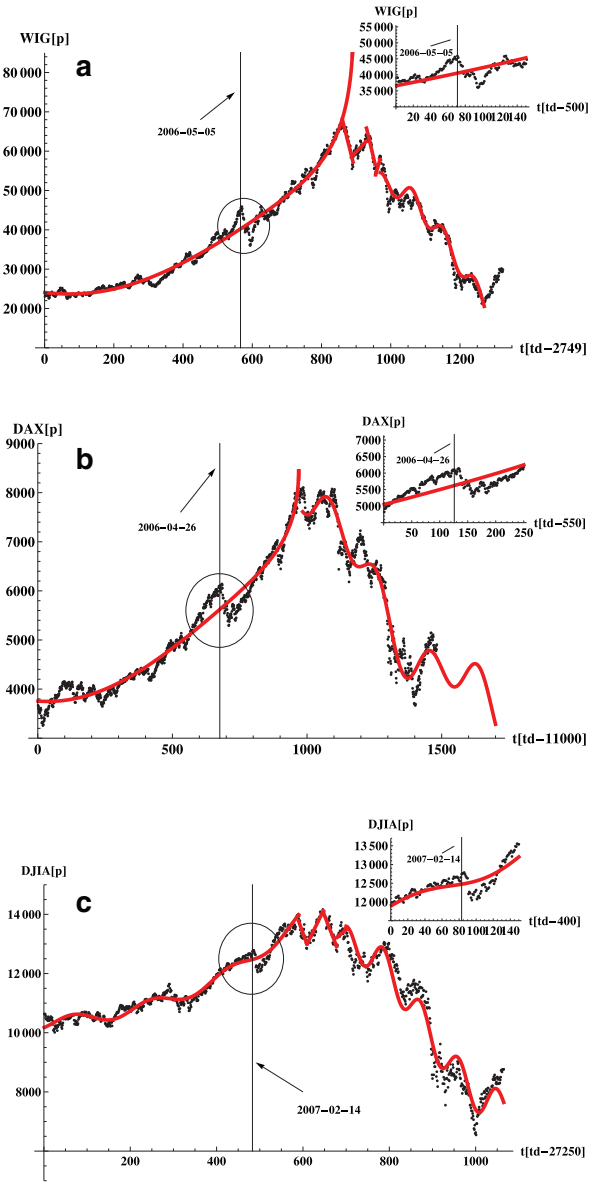

Fig. 1. Well-formed empirical peaks (the bubbles defined by erratic curves) of: (a) WIG index beginning on 6 February, 2004 (the –269th (=2480–2749)) trading day (td) on the Warsaw Stock Exchange) and ending on 18 May, 2009 (the 1326th(=4075–2749) td), (b) DAX index beginning on 6 February, 2004 (the -269th(=2480–2749) td) trading day (td) on the Frankfurter Wertpapierbörse and ending on 18 May, 2009 (the 1326th (=4075–2749) td), and (c) DJIA index beginning on 16 March, 2005 (the 27251st td on the New York Stock Exchange) and ending on 9 June, 2009 (the 28315th td). The solid curves represent the best theoretical long-term (multi-year) trend [25], defined by Eq. (A.1), found from the fit to the bull market (left-hand side of the peak). The thin solid vertical line denotes the position of the local maximum placed for: (a) 2006-05-05 (the 576th(=3325–2749) td); (b) 26 April, 2006 (the 676th(=11676–11000) td); and (c) 14 February, 2007 (the 483rd(=27733–27250) td). These maxima belong to the zigzags marked by the circles. These zigzags are emphasized by the inset plots, as they are the main subject of interest to us. Strongly oscillating trends (also solid curves) for bear markets (the right-hand side of the peaks) are plotted only for completeness.

The content of the paper is as follows. Section 2 is devoted to the empirical analysis of daily data originating from three typical stock markets of small, mid and large capitalisations. In Section 3, we explain how indicators arise when the system approaches a catastrophic bifurcation threshold. Section 4 contains concluding remarks. Detailed supplementary methodological considerations are presented in the appendices.

2. Analysis of empirical data

2.1. Time series and detrending

The conceptual strategy of our approach is separately to consider the deterministic components of both the trend and the drift effects, which makes viable the analysis of determinism contained in the empirical time series. We also assume that the detrending of the time series eliminates non-stationarity.

The analysis of empirical data we perform on the bubbles (peaks) of WIG, DAX and DJIA indices covers the 2007-08 worldwide financial crisis (cf. the erratic curves in Fig. 1(a), (b), (c)). The shapes of WIG, DAX, and DJIA peaks are strikingly similar. This suggests an underlying generic dynamical behaviour of European stock market evolution. In particular, the shape of bull markets (or booms) represented by the left-hand side of these peaks appears to be typical on stock exchanges of small to large capitalisations, as they contain very characteristic zigzags (denoted by circles). These bull markets are the principal subject of interest to us.

In order to model the deterministic long-term (multi-year) trend of these empirical bull markets – an observable long-term deterministic pattern in the empirical data caused by the herd effect,[3] we here use an easily interpretable relaxation function defined by Eq. (A.1), which is a solution to a dynamic equation describing the relaxation of a viscoelastic market ('biopolymer') (cf. Appendix A and [26]).

The trend and the drift each have different physical origins and operate at various time horizons, which makes their determination and analysis tractable. However, a generic problem of the decomposition of the deterministic part of time series for trend and drift components in a *unique* way is beyond the scope of this work and remains an open problem. Instead, we accept *some* level of trend (here given, by Eq. (A.1) – see Appendix A for details) if the coefficient of determination R^2 and the P-value assume the best values in comparison with the corresponding ones obtained from the fits of alternative trend functions.[4]

[3] Trend (e.g. the price trend) results from the feedback mechanism between traders and the market, which can therefore be considered to be a complex self-organizing system [24] and refs. therein.

[4] A complementary popular candidate for the trend, also having a well-interpreted physical origin, is the log-periodic oscillation ([24] and refs. therein). However, for empirical bull markets in our data, it is worse than the fit of the trend model used by us, which has a smaller R^2 (expressed, as usual, as the ratio of the explained (theoretical) variance to the sample variance). Notably, R^2 is the measure of concordance most often used. Unfortunately, all hitherto known trends are nonuniversal and can be applied only to well-defined long-term bubbles. Also trends given in the

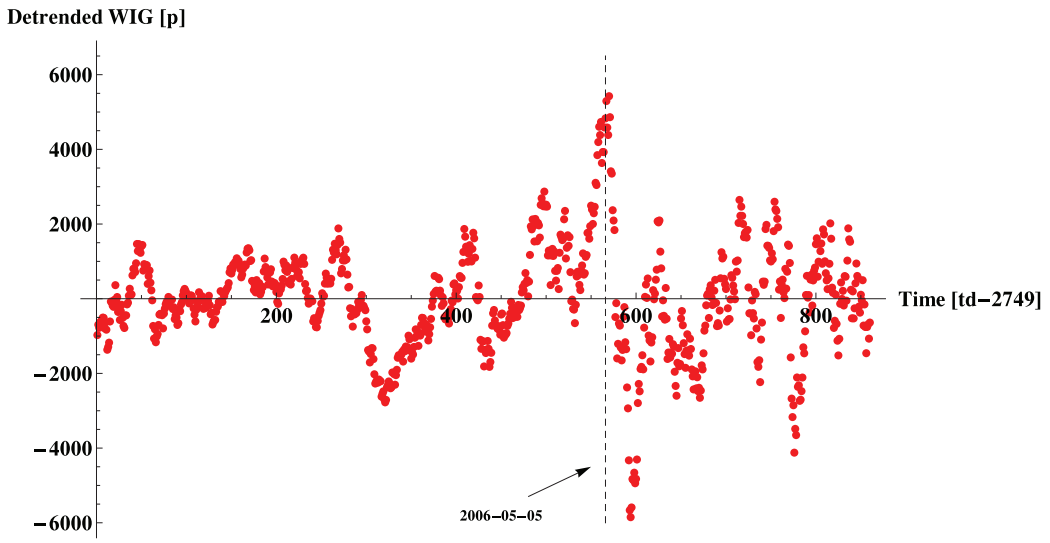

Fig. 2. The detrended time-dependent index WIG (the time series of WIG or the process x_t measured in points [p]), which constitutes the basis for further considerations. The characteristic date when the process x_t assumes its largest value is denoted by the vertical dashed line. The same date also defines the position of the index WIG's local maximum (cf. Fig. 1 (a)). The remaining indices (DAX and DJIA) show analogous behaviour and therefore, they are not presented in the figure.

By subtracting the trend (A.1), we obtain the detrended time series (cf. Fig. 2) consisting of the deterministic drift and noise – the extraction of the drift component from the time series and its systematic analysis are essential for our purpose.

2.2. Variance of detrended time series

For our three different time series, the time dependence of sufficiently sensitive estimators of variance, defined within the moving (or scanning) time window of one month width (or twenty trading days[5]) is shown in Fig. 3. That is, we obtained these estimators from the corresponding separate scans of the empirical time series. These scans were made by using the above-mentioned time window of fixed width and also a fixed scanning time step (again of one trading month). Indeed, within this window the variance estimator was calculated separately for each temporal position of the time window.

Notably, the variance estimators of time series show a sudden strong increase in the range of downturns (marked by the circles in Fig. 1), creating local peaks of these estimators in the form of spikes (cf. three plots in Fig. 3). The centres of these spikes are indicated in the plots by the vertical dashed lines. The existence of a spike is one of the principal empirical symptoms of a catastrophic (or possibly even critical) slowing down. Henceforth in the text, we refer to these spikes as catastrophic spikes.

Catastrophic spikes are preceded by well-formed local peaks of variance estimators of much smaller amplitude (cf. Fig. 3). This behaviour clearly manifests the so-called flickering phenomenon [48]. This effect can happen, for instance, if the system enters the intermediate bistable (bifurcation) region placed between two tipping points. Subsequently, the system stochastically moves up and down, either between the basins of attraction of two alternative attractors, or between an attractor and a repeller. The two possibilities are defined by stable/stable or stable/unstable pairs of equilibrium states. Such behaviour can also be considered to be an early warning of catastrophe. The flickering of the variance estimator (although less intense), together with intermittencies shrinking in time, is observed for even earlier time intervals (cf. the upper plot in Fig. 3). The flickering phenomenon is considered in detail in Sections. 2.3 and 2.4.

2.3. Recovery rate

As typical behaviour, Fig. 4 plots detrended time series element or process x_t against the preceding detrended time series one, x_{t-1}, for instance, for the (detrended) time-dependent WIG index. Two plots of short (one-month) subseries of essentially different empirical data sets are shown in Fig. 4 as an example. Each subseries consists of 20 successive pairs of elements (x_{t-1}, x_t) extending from $t = 502$ to $t = 521$ [td-2749][6] trading days (black circles) and from $t = 542$ to $t = 561$ [td-2749] trading days (red inverted triangles), respectively. The slopes of the straight lines, fitted separately to both data sets, give two different values of the linear or the first-order autoregression coefficient $AR(1)$. Hence, these slopes give values of coefficient $\lambda = AR(1) - 1$, where λ is a derivative of the

form of polynomials, quite often used in econometry, result in worse statistic characteristics of the fits in our data.

[5] Twenty trading days is considered to be one trading month. The risk-free period of the Central Bank is likewise one month.

[6] This notation means that the origin of coordinates of plot (a) is shifted by 2749 [td] relative to the beginning of quotation on the Warsaw Stock Exchange. Analogous situations concern German Stock Exchange (plot (b)) and NYSE (plot (c))

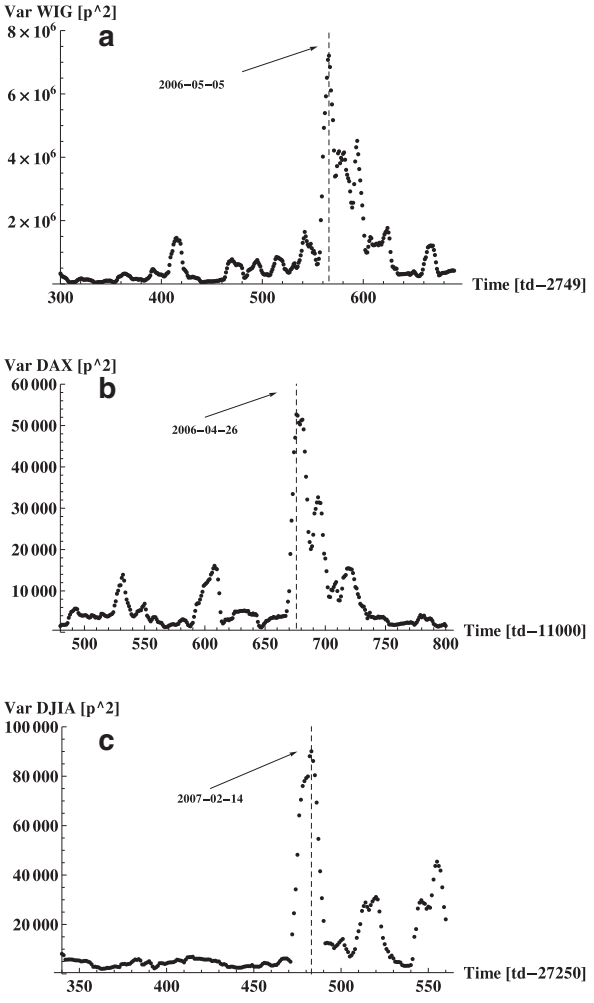

Fig. 3. Plots of the variance estimators of the detrended indices – time series of WIG, DAX and DJIA (these time series are shown in the three corresponding plots in Fig. 2). Here, the time ranges from 2005-04-15 to 2006-11-15 for WIG (plot (a)), from 2005-08-18 to 2006-10-19 for DAX (plot (b)), and from 2006-07-21 to 2007-05-09 for DJIA (plot (c)). The vertical dashed lines denote the positions of the spikes' centres.

nonlinear drift term, $f(x_t; P)$ (here P is a driving or control parameter), over the time series variable, x_t, at a fixed point x^*, present in the linearized discrete stochastic dynamic Eqs. (B.6) and (B.7). This linearization is a generic property of the system which has a fixed point or contains an equilibrium (stable or unstable). These equations are valid in the vicinity of any fixed point, in particular, in the vicinity of the most interesting tipping point (or the catastrophic bifurcation threshold – cf. Appendix B). Furthermore, different values of the shift coefficient $b(=A(0)$, being a zero-order autoregression coefficient), although relatively small, are well distinguishable in the inset plot.

From the fits mentioned above, $AR(1)$ coefficient almost equal to 0.95 is found (cf. the slope of the red solid straight line, shown in Fig. 4, fitted to the red inverted triangles – this corresponds to the time interval ranging from $t = 542$ to $t = 561$ [td-2749] shown in Fig. 5(a)) for the subseries

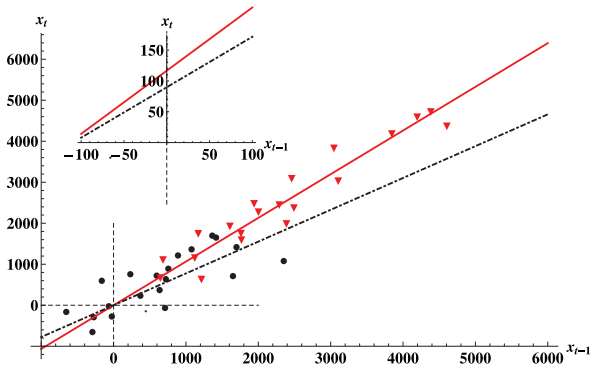

Fig. 4. The detrended successive WIG time series x_t vs. x_{t-1} for twenty pairs (or one month) ranging from $t = 502$ to 521 [td-2749] (black circles and fitted black dotted-dashed straight line) and from $t = 542$ to 561 [td-2749] (red inverted triangles and fitted red solid straight line) time steps. The slopes of the fitted curves, i.e. autoregressive coefficient of the first-order $AR(1)$, almost equal 0.65 and 0.95, respectively. These results give $-\lambda \approx 0.35$ and $-\lambda \approx 0.05$, respectively. (See also plot (a) in Fig. 5.) Furthermore, respective values of the shift coefficient or autoregressive coefficient of the zero-order $b = A(0)$, although relatively small, are well distinguishable in the inset plot at $x_{t-1} = 0$. For interpretation of the references to colour in this figure legend, the reader is referred to the web version of this article.

immediately before the catastrophic bifurcation threshold (marked by the dashed vertical straight lines plotted in Figs. 2, 3 and 6, and by thin vertical lines in Fig. 1). In Fig. 5(a) this slope gives the $-\lambda$ represented by the blue dot with error bar placed at time $t = 561$ [td-2749] on the left-hand side of the catastrophic bifurcation threshold. The black dashed straight line is shown for comparison in Fig. 4, having a distinctly lower slope $AR(1) \approx 0.65$, which corresponds to the time interval ranging from $t = 502$ to $t = 521$ [td-2749]. Hence, the corresponding $-\lambda \approx 0.35$ is represented in the same figure by the blue dot with the error bar placed at time $t = 521$ [td-2749], also on the left-hand side of the catastrophic bifurcation threshold. The origin of the red dots (without error bars) obtained using a complementary approach is described below.

In Appendix B, we prove that the autocorrelation function of the hth order, $ACF(h)$, is expressed by the formula given in the second row in (B.10). In fact, we here study a particular case of $ACF(1) = AR(1)$ by a method complementary to that used above for the analysis of the coefficient $AR(1)$. Namely, we apply the usual estimator, $ACF_{EST}(1)$, of $ACF(1)$ for a given month (which is our time window where λ is an almost constant value),

$$ACF_{EST}(1) = \frac{1}{Var(x_t)}\frac{1}{T} \times \left[\left(\sum_{t=1}^{T} x_t\, x_{t+1}\right) - \frac{1}{T}\left(\sum_{t=1}^{T} x_t\right)\left(\sum_{t=1}^{T} x_{t+1}\right)\right], \quad (1)$$

where $T = 20$. Using this estimator, $-\lambda$ is calculated and presented in Fig. 5 by the red dots (without error bars), which almost everywhere fall within the error bars, thus their time dependence is qualitatively similar, as expected. This result, together with the corresponding one for the

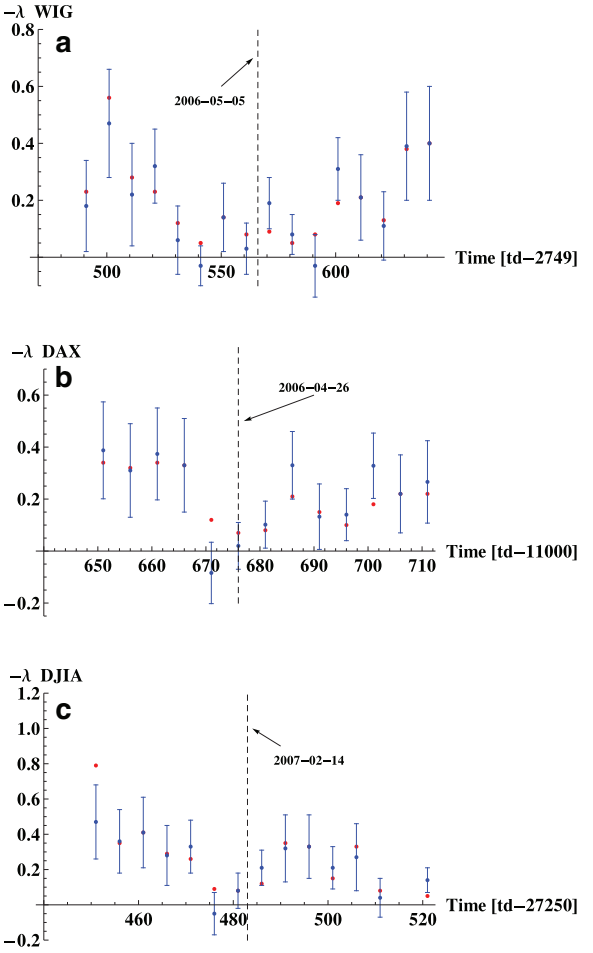

Fig. 5. The recovery rate $-\lambda(\geq 0)$ vs. time calculated by using two different formulas: (i) $-\lambda = 1 - AR(1)$ (blue dots with error bars) and (ii) $-\lambda = 1 - ACF(1)$ (red dots without error bars). The two curves have similar shapes in time (they are concave where data resolution equals 2 [td] to make the plots better visible) having local minima for $-\lambda \approx 0.0$. As these minima are reached from their positive sides, such a behaviour leads to the slowing down of the system's return to the stable equilibrium (see Appendix B for details). The vertical dashed lines denote in plots (a), (b), and (c) (as usual) the position of tipping points. For interpretation of the references to colour in this figure legend, the reader is referred to the web version of this article.

coefficient $AR(1)$ (shown by blue dots with error bars in the same figure), is necessary to calculate equilibrium states (stable and unstable) defined in the next paragraph by the set of x^* values.

The empirical data shown in Fig. 5 provide the recovery rate, $-\lambda$, "smiles" with heights of minimums equal zero (to a good approximation). Notably, the most significant result is that the minimum of both curves is located at the same place, having (to good approximation) the same height. Some small differences between the two curves can (from this point of view) be neglected, particularly as we can roughly expect that red dots have error bars of the same order as blue dots. Indeed, the minimum of $-\lambda$ is the source of a slowing down effect (see Appendix B for details). This effect is one of the necessary requirements

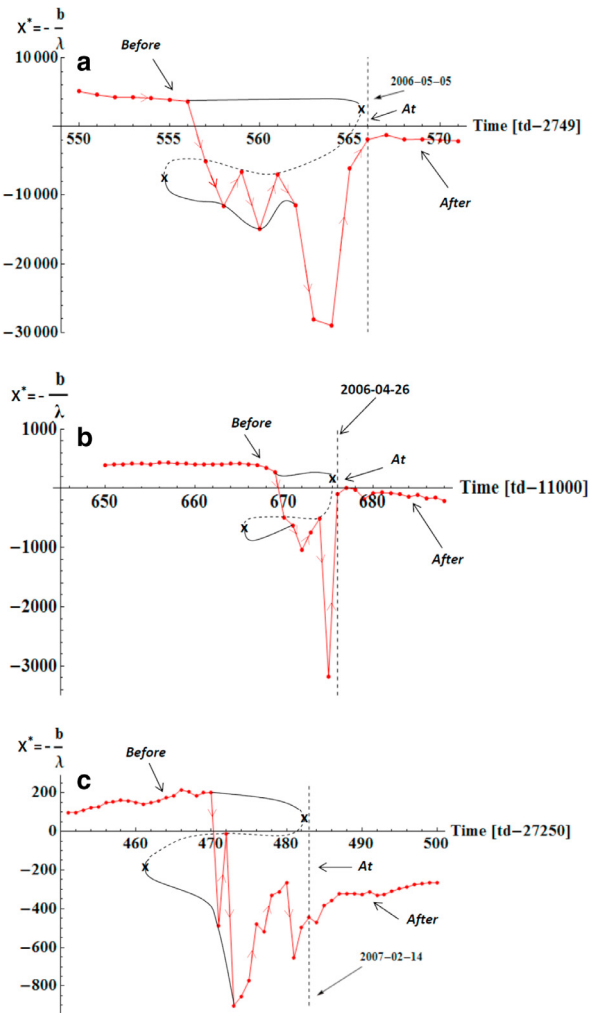

Fig. 6. Empirical curves (small red circles joined by the segments of red lines presented in plots (a), (b), and (c)), representing the (mechanical) equilibrium states defined by the values of $x^*(=-b/\lambda)$ vs. time (in trading days, td), where b and λ were obtained from the empirical data for WIG, DAX, and DJIA (cf. Figs. 4 and 5). The flickering phenomenon, present prior to the catastrophic bifurcation threshold, is illustrated by the red curve directed by arrows which oscillate up and down between red empirical data points located alternately on the dotted and solid black curves. This threshold is marked by the dashed vertical line indicated by an arrow termed 'At'. The upper segment of the backward-folded curve is the solid one – initially red with dots and then black. It is indicated by the arrow termed 'Before' and drawn schematically until the right tipping point denoted by the character 'x' (placed one day before the catastrophic bifurcation threshold). This upper segment is identified as a sequence of stable (mechanical) equilibrium states of the type $x^*_{1''}$ (see Appendix C and Figs. 8–11 for details). The segment (denoted by the dotted curve) placed in the bistable region between two tipping points (the left tipping point is also denoted by the character 'x') consists of a sequence of unstable (mechanical) equilibrium states of the type $x^*_{1'}$ (see Appendix C and Figs. 8–11 for details). The lower segment (also denoted by the solid curve - initially black and then red) placed after the left tipping point is identified as a complementary sequence of the stable (mechanical) equilibrium states, here of x^*_1 type (its part after the catastrophic bifurcation threshold is indicated by the arrow and termed 'After'; see Appendix C and Figs. 8–11 for details). Remarkably, the dotted curve can be smoothly plotted between the two tipping points and over the empirical points. (An explanation about the construction of the backward folded curve is given in paragraph 2.4). For interpretation of the references to colour in this figure legend, the reader is referred to the web version of this article.

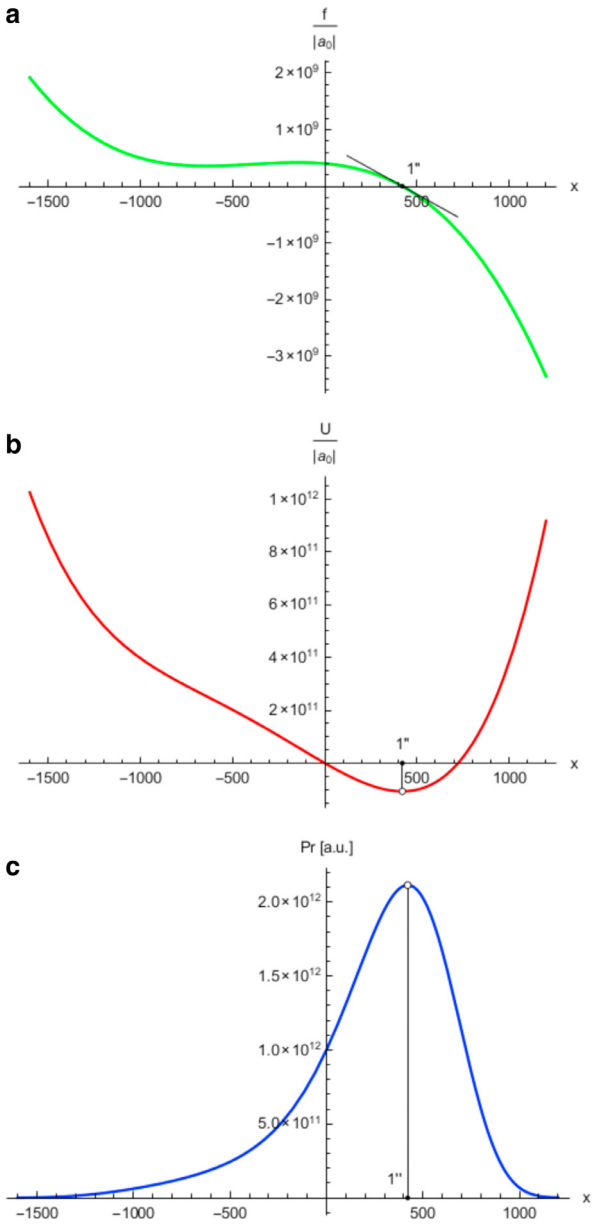

Fig. 7. Three complementary plots concerning the same region placed before the first tipping point of the backward-folded curve (or empirical data, for instance, for DAX) denoted in Fig. 6(b) by the character 'x'. The (mechanical) equilibrium point $1''(=x^*_{1''}) = 421.009$, shown in the upper plot (a) as the single root of the equation $f(x;P)=0$, is obtained directly from the empirical data (– the ordinate of this root shown in Fig. 6(b) is the time = 665 [td-11000]). The upper plot (a) shows the dependence of the force $f(x;P)$ (present in Eqs. (B.1) and (C.2)) vs. x for the values of (relative) coefficients a_1/a_0=1179.81, a_2/a_0=278390 and a_3/a_0=-4.00948 × 10^8 obtained in the C.4 ('Case before the bistable region') and common to all the plots (a), (b), and (c). In the middle plot (b) the corresponding potential, $U(x;P)$, is shown where the point 1" is the sole stable equilibrium. In the bottom plot (c), the equilibrium probability distribution, $Pr(x;P)$, given by Eq. (B.5), is shown. Notably, variable x equals x^* only if x becomes a root of f. For interpretation of the references to colour in this figure legend, the reader is referred to the web version of this article.

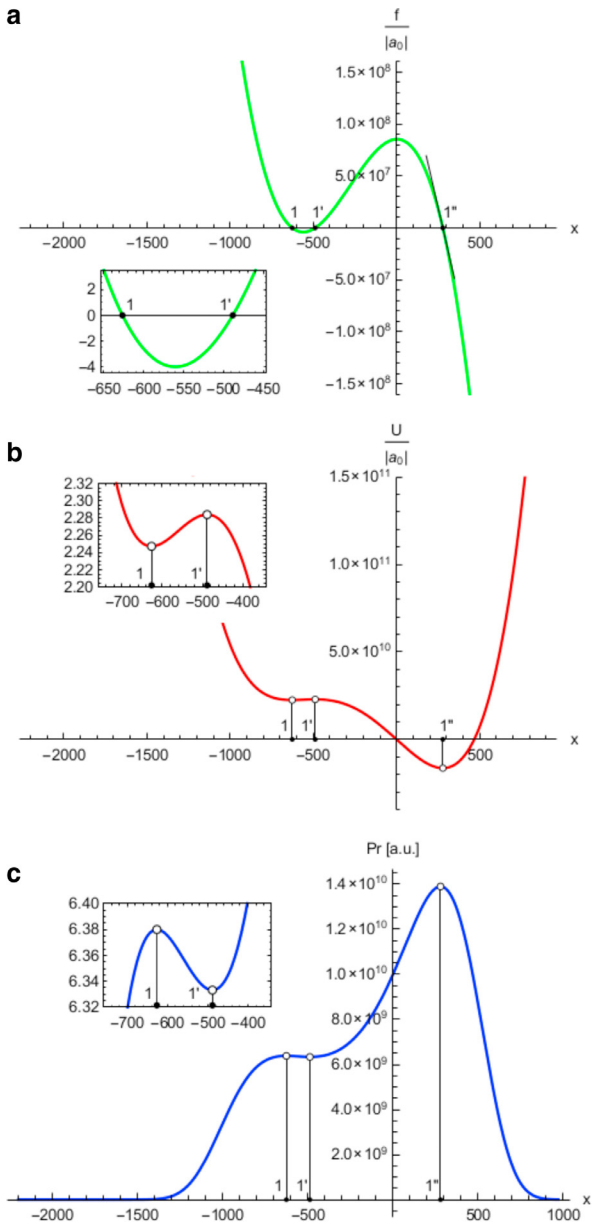

Fig. 8. Three complementary plots concerning the same bifurcation (bistable) region (denoted by the arrow 'Before' in Fig. 6(b)) ahead of the catastrophic bifurcation threshold, denoted there by the vertical dashed straight line. The (mechanical) equilibrium points x^*_1 = -626.473, $x^*_{1'}$ = -488.308 and $x^*_{1''}$ = 278.92, as roots of equation $f(x;P)=0$ (see Appendix C for details), are obtained directly from the empirical data (or backward-folded curve) shown there. The ordinates of these points (shown in Fig. 6(b)) are times = 669, 670, and 671 [td-11000], respectively. The upper plot (a) shows the dependence of the force, $f(x;P)$, (present in Eq. (B.1)) vs. x for the values of the relative coefficients a_1/a_0 = 835.861, a_2/a_0 = -5022.94 and a_3/a_0=-8.53249 × 10^7 obtained in the C.2 ('Case of the bistable region') common to all the plots (a)–(c). In the middle plot (b) the corresponding bistable potential, $U(x;P)$, is shown. The points 1 and 1'' are stable equilibria, while 1′ is an unstable one (hence, $\Delta x_{1,1''} = 905.393$). In the bottom plot (c) the bistable equilibrium probability distribution, $Pr(x;P)$, given by Eq. (B.5) is shown. The inset plots better visualize the behaviour of f, U and Pr vs. x in a very restricted region containing the points 1 and 1′. Notably, variable x equals x^* only if x becomes a root of f. For interpretation of the references to colour in this figure legend, the reader is referred to the web version of this article.

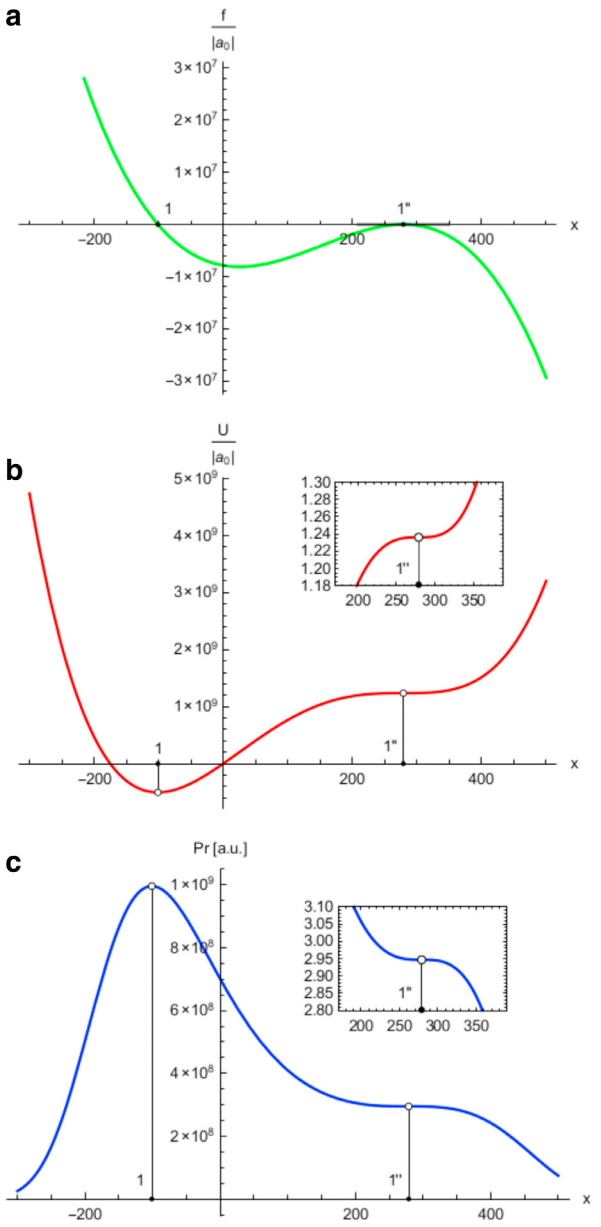

Fig. 9. Three complementary plots concerning the same bifurcation (bistable) region at the catastrophic bifurcation threshold; the region is denoted by the arrow 'At' in Fig. 6(b). All the curves are plotted for the same values of the relative coefficients $a_1/a_0 = -456.67$, $a_2/a_0 = 21359.70$ and $a_3/a_0 = 7.87066 \times 10^6$ derived in C.1 ('Case of the catastrophic bifurcation transition') from the zeros of the $f(x; P)$ curve. Apparently, the curve $f/|a_0|$ vs. x in the upper plot (a) has a single twofold root $x^*_{1'} = x^*_{1''} = 278.92$ (– the ordinate of this root shown in Fig. 6(b) is the time = 675 [td-11000]). This root, being the second tipping point, is denoted in Fig. 6 by the character 'x' and placed in the immediate vicinity of the threshold. The first root $x^*_1 = -101.17$ is given directly by the empirical point placed on the threshold shown in Fig. 6(b) (hence, $\Delta x_{1,1''} = 380.09$). In the middle plot (b) the corresponding bistable potential, $U(x; P)$, is shown (for the same relative coefficients as for the upper plot). The points 1 and 1'' are stable equilibria. In the bottom plot (c) the bistable equilibrium probability distribution, $Pr(x; P)$, given by Eq. (B.5), is shown. The inset plots better visualize the behaviour of f, U and Pr vs. x in a very restricted region containing the point 1''. Notably, variable x equals x^* only if x becomes a root of f. For interpretation of the references to colour in this figure legend, the reader is referred to the web version of this article.

(or signatures) for the existence of a phase transition, in particular, of the catastrophic bifurcation type.

Our approach is justified by assuming that λ is a piecewise, almost constant function of time, i.e., it is an almost fixed quantity for the monthly set of empirical data points. We assume the same for the shift coefficient b considered below. Hence, λ and b are slowly varying functions of time (counted in months) in comparison with the process x_t (counted in days). The difference in these two time scales plays a basic role in our considerations.

2.4. Empirical catastrophic bifurcation transitions

The shift coefficient b relates to the recovery rate $-\lambda(> 0)$ and fixed point (root) x^* through the key equality $b = -\lambda x^*$ (see the second Equation in (B.7)). Hence, x^* is plotted vs. time in Fig. 6 for three typical indices: (a) WIG, (b) DAX, and (c) DJIA. Apparently, sufficiently far before the catastrophic bifurcation threshold (denoted by the vertical dashed straight lines in plots (a), (b), and (c)) and after it, the spontaneous reduction of error bars of the curve x^* vs. time (t) is observed together with the smoothing out of two substantially extended segments of this curve denoted by the terms 'Before' and 'After', which can be identified as two evolving separable equilibrium states of the system. The significant jumps of empirical data points (leading to system instability) are seen solely within the region between these two. The range of instability is defined for plot (a) by empirical points placed between time $t = 557$ and $t = 565$, for plot (b) between time $t = 670$ and $t = 674$, and for plot (c) between time $t = 471$ and $t = 482$. These empirical facts are apparently of a rather universal nature, as they are consistently observed on typical stock markets of small, mid and large capitalisations.

The structure of the unstable region enables us to outline the backward folded curve – both its stable and unstable segments – which exposes the so-called flickering phenomenon. Positions of both tipping points (denoted by the character 'x') are defined solely schematically (in crude approximation) to better indicate the folding effect. Although the location of the right tipping point is defined with one-day precision, the location of the left tipping point has about three days' uncertainty. The vertical uncertainty of both tipping points can be assumed to be no greater than about 2000 to preserve the smooth character of the backward folded curve. That is, all backward folded curves, which could be drawn to serve as non-analytical eye guides, should be topologically equivalent. Therefore, it is possible to construct the backward folded eye-guide curves together with their tipping points as they are sufficiently limited by the spatial constraints.

As indicated above, the precise location of the tipping points is of no importance to us. What is important is solely the specific structure (shape) of the backward-folded curve, which propels the dynamics over the unstable region. Indeed, the unstable segment of this curve consists of a sequence of states responsible for the flickering phenomena that is, for large oscillations across these states – in the case of the absence of an unstable segment, the flickering phenomena would be suppressed.

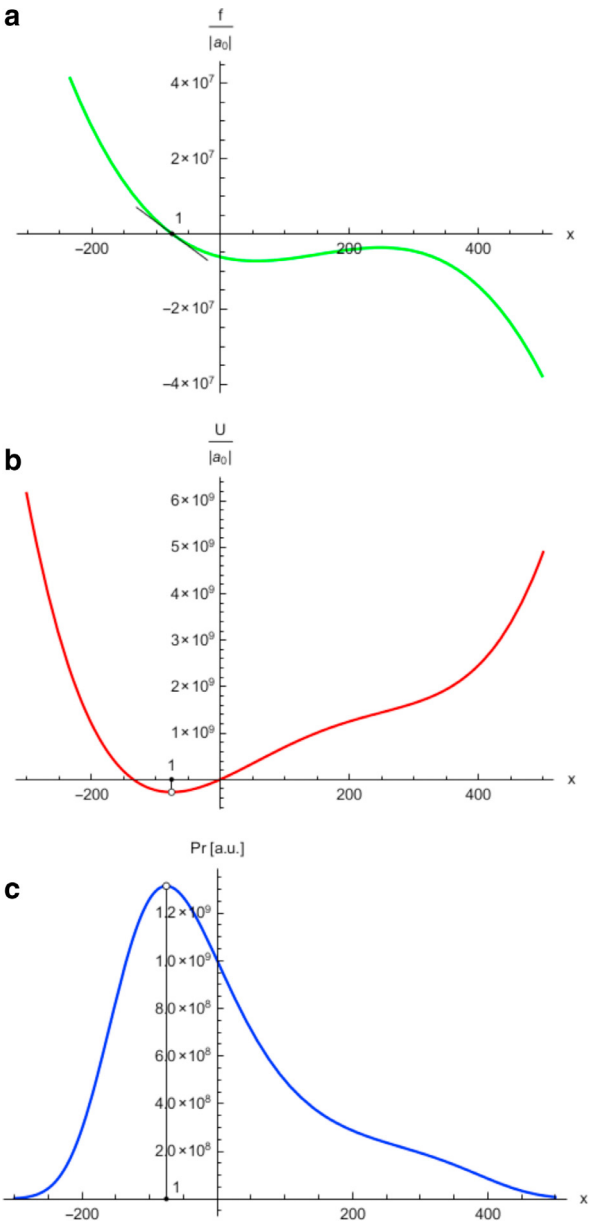

Fig. 10. Three complementary plots concerning the same region after the bifurcation (bistable) threshold (denoted by the vertical dashed straight line); the region was denoted in Fig. 6(b) by the arrow 'After'. All the curves were plotted for the same values of the relative coefficients $a_1/a_0 = -456.67$, $a_2/a_0 = 41709.50$ and $a_3/a_0 = 6.1682 \times 10^6$ derived in C.3 ('Case after the catastrophic bifurcation transition') from the zeros of $f(x; P)$ curve obtained from the empirical data shown in Fig. 6(b). The curve $f/|a_0|$ vs. x in the upper plot (a) has a single root $x_1^* = -75.39$ (– the ordinate of this root shown in Fig. 6(b) is the time = 680 [td-11000]). In the middle plot (b) the corresponding potential, $U(x; P)$, is shown. Point 1 is a stable equilibrium. In the bottom plot (c), the equilibrium probability distribution, $Pr(x; P)$, given by Eq. (B.5), is shown. Notably, variable x equals x^* only if x becomes a root of f. For interpretation of the references to colour in this figure legend, the reader is referred to the web version of this article.

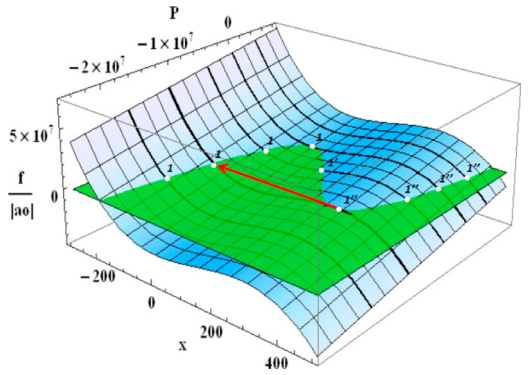

Fig. 11. A comprehensive three-dimensional schematic view showing the origin of the flat backward-folded curve x^* vs. P placed on a (semi-transparent) green plane. This backward-folded curve originated as a section of the green plane with the wavy blue surface. The points denoted by 1 and 1′′ (white circles) are stable mechanical equilibria located, respectively, on the left and right segments of this curve. The points denoted by 1′ (also white circles) are unstable mechanical equilibria located on the backward-folded segment of this curve. The catastrophic bifurcation transition from the equilibrium state 1′′ to 1 is indicated by the long red arrow. These particular points are placed on the catastrophic bifurcation curve (thicker than all other curves) located on the wavy blue surface. Note, that the singular behaviour of the schematic backward-folded curve in the vicinity of the catastrophic bifurcation threshold (cf. in plots (a), (b), (c) in Fig. 6) is absent here. The impact of the noise η_t on the states x_t and x_t^* is not visualized here. Notably, variable x becomes x^* only if x becomes a root of f. For interpretation of the references to colour in this figure legend, the reader is referred to the web version of this article.

Flickering is well pronounced in Fig. 6, ahead of the negative catastrophic spikes evident in plots (a), (b), and (c) and defining the bistable regime. This flickering phenomenon appears within the bistable region, where the sequence of unstable (intermediate) states or roots $\{x_{1'}^*\}$ (see Appendix B and Appendix C for details) placed on the hypothetic (dotted) curve causes the system to bounce between these states and the sequence of stable states $\{x_1^*\}$ indicated on the hypothetical lower (solid) curve. Indeed, this *bounce* effect can cause, for instance, oscillations in the variance ahead of the spikes shown in plots (a), (b), and (c) in Fig. 3. We consider the existence of the flickering phenomenon and subsequent spike between two rather flat sequences of states as a possible result of a catastrophic bifurcation transition. This is discussed in detail in B.3 (see Eq. (B.13)). It should be emphasized that the three-phase sequence observed: 'equilibrium–instability (or flickering)–equlibrium' during the system evolution is essential for the formulation of a sound conjecture of the bistability or dynamic bifurcation.

The results shown in Fig. 6 constitute the basis for further discussion because they suggest that bifurcations or bistabilities on financial markets can exist. Thus, they validate considering the trajectory of $x^*(t)$ as extrema (minima or maxima) of a hypothetical 'mechanical' potential curve (drawn in the third dimension, i.e. along the third (vertical) additional axis which can be attached to plots (a), (b), and (c) in Fig. 6).

3. Mechanical-like view

Following the article by [17] and by using basic results presented in Fig. 6, we provide a quantitative description founded on the mechanical-like picture of a ball moving in the potential landscape. We consider snapshot pictorial views of different states of the system on the pathway to regime change illustrated by a sequence of properly chosen Figs. 7–11. This pathway is defined by dependence $x^* = x^*(P)$, where the driving (hidden) parameter P is, by definition, a slowly-varying function of time (see Appendix C for a detailed expression). The point x^* is a root of equation $f(x; P) = 0$ – see the respective zeros 1, $1'$ or/and $1''$ shown (by small black circles) in the upper plots (a) of the force $f(x; P)$ vs. x in Figs. 7–10, and also the sequence of points 1, $1'$ and $1''$ (white circles) present in the summary of Fig. 11. In the middle plots (b) the potential $U(x; P)$ vs. x is shown, indicating that the points 1, $1''$ are stable, while point $1'$ is unstable. Finally, in the bottom plots (c), the equilibrium probability distribution, $Pr(x; P)$ given by Eq. (B.5) is shown versus x. Figs. 8 and 9 show the most significant results of our work, namely both a bifurcation (cf. Fig. 8) and a catastrophic bifurcation (cf. Fig. 9) observed in empirical financial time series.

Let us examine the pathway to regime change with greater care. When time increases, the system passes successive states defined by the values of x^*, well pronounced in Fig. 6. The initial characteristic state defined by a single value of x^* is shown in Fig. 7. It represents the region ahead of the bifurcation. The central objective of interest to us is defined in Fig. 8 by the three different values of x^*. The borders of the bifurcation region, limited by tipping points, are denoted in the plots in Fig. 6 by the character 'x'. The arrows show the possible transitions between the equilibrium points. The third, extremely interesting case of the catastrophic bifurcation transition is presented in Fig. 9. For this case, the points $1'$ and $1''$ coincide. The point $x^*_{1''}$ is represented in Fig. 6 by the second character 'x'. In this case, the possible transition between the points $1''$ and 1 is shown schematically by the arrow in Fig. 11. The last (fourth) case, illustrated by Fig. 10, is similar to the first one, as again it is defined by a single root, namely by 1.

Notably, the two segments of the folded backward curve $x^*(P)$ containing the points 1 and $1''$ (cf. Fig. 11) represent stable equilibria, while the third backward segment in between, containing the points of the $1'$ type, represents an unstable equilibrium. If the system is driven slightly away from the stable equilibrium it will return to this state with the relaxation time $\tau(P) = -1/\lambda(P)$ (cf. considerations in Appendix B in particular Eq. (B.9)). Otherwise, the system driven from the unstable equilibrium will move away (to one of the two stable equilibria). In fact, the backward segment of the curve $x^*(P)$ (denoted by the dashed backward curves in the plots in Fig. 6) represents a border or a repelling threshold between the corresponding basins of attraction of the two alternative stable states (defined by the lower and the upper branches of the backward-folded curves, marked in the same figures by the solid curves).

In this work, we focus mainly on the analysis of stable equilibria. Two of them are the tipping points at which a tiny perturbation (spontaneous or systematic) can produce a sudden large transition (indicated, e.g. for the second tipping point, by a long arrow in Fig. 11). It should be noted that only in the vicinity of the stable equilibria, that is for the points placed on the lower or the upper branches of the folded curve, the variance of the detrended time series diverges according to a power-law (cf. Expression (B.11) in Appendix B). This is a direct consequence of the catastrophic slowing down (CSD), which can be well detected before the actual occurrence of the catastrophic transition. This divergence can be intuitively understood as follows. As the return time diverges, the impact of a shock does not decay (see solution Eq. (B.9)), and its accumulating effect increases the variance. Hence, CSD reduces the ability of the system to follow the fluctuations [48].

We explain in this Section how indicators (or early warnings) arise when the system approaches the regime shift or the catastrophic bifurcation transition (threshold). It is sufficient to consider the linear early warnings such as variance, recovery time, reddened power spectra and related quantities in the framework of the linearized theory defined by Eqs. (B.6) and (B.7). It is convenient to consider the nonlinear indicators (such as a non-vanishing skewness) by the approach based on the nonlinear and asymmetric part of the force $f(x; P)$ (present in the first equality in (B.1)) and on its asymmetric potential $U(x; P)$ (present in the second equality in (B.1)), both in the immediate vicinity of the regime shift – cf. plots in Fig. 9 concerning the case at the catastrophic bifurcation threshold.[7] This is one of the simplest viewpoints considered, for instance, in the article by Guttal and Jayaprakash [17].

4. Concluding remarks

Following the supposition in [29] concerning the possibility of the existence of bifurcation transitions, in particular catastrophic ones, on financial markets, we have studied the principal and most significant indicators of such transitions on stock exchanges of small and mid to large capitalisations. Other indicators (not visualized in this work) relating to properties of noise also confirm this supposition. All these indicators consistently show that the thresholds presented in Figs. 3, 5, 6, and 9 should be identified as signatures of a catastrophic bifurcation transition. It was a noteworthy surprise in our analysis that the catastrophic bifurcation threshold itself constitutes a consistent indicator in daily empirical data obtained from various stock exchanges. As we have observed, such a threshold – serving as an early indicator – is noticeable for several months before the global crash.

The basic results of this work consist of the well-established observations that: (i) λ is a negative quantity, and (ii) recovery rate $-\lambda$ vanishes when the system approaches the catastrophic bifurcation threshold (cf. Fig. 5). This vanishing effect (together with the result mentioned below, concerning the shift parameter b) permits us to for-

[7] Notably, the upper plot indicates that the maximal value of discontinuity of the recovery rate $-\lambda$ should exist at the bifurcation threshold. However, this value is too small to be recognized (as statistical errors are too large); cf. plots in Fig. 5.

mulate the hypothesis that the underlying phenomenon is a catastrophic (but not critical) slowing down. The significance of this result is furthermore underlined by the fact that λ is a fundamental quantity which (as we are able to prove) enters all other linear indicators and also participates in non-linear ones.

Apart from λ, we have also identified the shift parameter b (cf. Fig. 4 and, in particular, the insert figure presented there). Hence, we have been able to present an empirical trajectory consisting of fixed points x^* plotted vs. trading time t, and directly observe the catastrophic bifurcation transition preceded by the flickering phenomenon (cf. plots in Figs. 6). Furthermore, we have found that each catastrophic bifurcation transition is preceded by a singularity-like anti-peak, which appears to be a super-extreme event (see again the plots in Figs. 6). As a consequence, we have been able to construct a mechanical-like view of the bifurcation transitions, resulting in a bimodal shape of the (unconditional) equilibrium statistics[8] (see Figs. 8 and 9 for details).

Our contribution opens possibilities for numerous applications, for instance for forecasting, market risk analysis and financial market management. In addition, the approach stimulating our present work is derived in part from ecology [17,48,50,52], where sometimes an ecosystem undergoes a catastrophic regime shift (in the sense of the Réne Thom catastrophe theory [17] over a relatively short period of time. Hence, this opens the possibility for the methodological elements of our work to be applicable in such domains. Nevertheless, a word of warning is in place here, as one can easily deceive oneself by seeing deterministic dynamics at work in random data with a certain structure, as demonstrated for example in [31]. Criteria for validating the emergent nature of such structures can prevent this kind of over-interpretation, and devising such criteria constituted the main goal of this work.

Acknowledgments

We are grateful to Piotr Suffczyński for stimulating discussions. T.G., T.R.W., and R.K. acknowledge partial financial support from the Polish Grant No. 119 awarded in the First Competition of the Committee of Economic Institute, organized by the National Bank of Poland.

Appendix A. Detrending procedure

In order to model the long-term trend of the time series presented in Fig. 1, we used the following relaxation function of time t:

$$X(|t-t_c|) = (X_0+X_1)E_\alpha\left(-\left(\frac{|t-t_c|}{\tau}\right)^\alpha\right) - X_1\cos(\omega|t-t_c|)\cos(\Delta\omega|t-t_c|), \quad X_0,\alpha,\tau,t_c>0, \tag{A.1}$$

separately valid both for the bullish and the bearish sides of a given well-formed market bubble. (Predictions of Formula (A.1) are shown in Fig. 1 using solid lines.) Here, we have $\omega, \Delta\omega \ll 1$, as this is required in the theoretical derivation of the above equation; see [25] for details. All the parameters with the corresponding fitted values are listed in Tables A.1–A.12 .

[8] We can say that this observation is seen even better for WIG and DJIA than for DAX.

Table A.1
Values of fit parameters of the trend for WIG bull market ($R^2 = 0.9986$).

Parameter	Value	Standard deviation
t_c	892 [td]	73 [td]
τ	105 [td]	420 [td]
α	0.57	0.23
ω	0.0041 [td^{-1}]	0.0005 [td^{-1}]
$\Delta\omega$	0.0	0.0

Table A.2
Values of fit coefficients of the trend for WIG bull market ($R^2 = 0.9986$).

Coefficient	Value [p]	Standard deviation [p]
X_0+X_1	60081	85273
X_1	−8659	2352

Table A.3
Values of fit parameters of the trend for WIG bear market ($R^2 = 0.9985$).

Parameter	Value	Standard deviation
t_c	810 [td]	0 [td]
τ	272 [td]	20 [td]
α	1.562	0.025
ω	0.0431 [td^{-1}]	0.0005 [td^{-1}]
$\Delta\omega$	0.0065	0.0004

Table A.4
Values of fit coefficients of the trend for WIG bear market ($R^2 = 0.9985$).

Coefficient	Value [p]	Standard deviation [p]
X_0+X_1	41963	334
X_1	−2528	269

Table A.5
Values of fit parameters of the trend for DAX bull market ($R^2 = 0.9985$).

Parameter	Value	Standard deviation
t_c	969 [td]	1 [td]
τ	426 [td]	391 [td]
α	0.52	0.03
ω	0.00362 [td^{-1}]	0.00004; [td^{-1}]
$\Delta\omega$	0.0065	0.0004

Table A.6
Values of fit coefficients of the trend for DAX bull market ($R^2 = 0.9985$).

Coefficient	Value [p]	Standard deviation [p]
X_0+X_1	4698	82
X_1	−763	35

Table A.7
Values of fit parameters of the trend for DAX bear market ($R^2 = 0.9977$).

Parameter	Value	Standard deviation
t_c	968 [td]	0 [td]
τ	426 [td]	72 [td]
α	1.12	0.03
ω	0.0089 [td^{-1}]	0.0001; [td^{-1}]
$\Delta\omega$	0.0246	0.0001

Table A.8
Values of fit coefficients of the trend for DAX bear market ($R^2 = 0.9977$).

Coefficient	Value [p]	Standard deviation [p]
$X_0 + X_1$	5464	70
X_1	−847	36

Table A.9
Values of fit parameters of the trend for DJIA bull market ($R^2 = 0.9996$).

Parameter	Value	Standard deviation
t_c	627 [td]	3 [td]
τ	333 [td]	38 [td]
α	1.29	0.02
ω	0.0107 [td^{-1}]	0.0002; [td^{-1}]
$\Delta\omega$	0.0220	0.0002

Table A.10
Values of fit coefficients of the trend for DJIA bull market ($R^2 = 0.9996$).

Coefficient	Value [p]	Standard deviation [p]
$X_0 + X_1$	3486	40
X_1	−332	28

Table A.11
Values of fit parameters of the trend for DJIA bear market ($R^2 = 0.9971$).

Parameter	Value	Standard deviation
t_c	640 [td]	0 [td]
τ	165 [td]	191 [td]
α	1.938	0.575
ω	0.030 [td^{-1}]	0.070; [td^{-1}]
$\Delta\omega$	0.040	0.070

Table A.12
Values of fit coefficients of the trend for DJIA bear market ($R^2 = 0.9971$).

Parameter	Value [p]	Standard deviation [p]
$X_0 + X_1$	4010	110
X_1	−866	81

The Mittag-Leffler function $E_\alpha(\ldots)$ is defined as follows [35]:

$$E_\alpha\left(-\left(\frac{|t-t_c|}{\tau}\right)^\alpha\right) = \sum_{n=0}^{\infty} \frac{(-1)^n}{\Gamma(1+\alpha n)}\left(\frac{|t-t_c|}{\tau}\right)^{\alpha n}. \quad \text{(A.2)}$$

Here t_c denotes the localization of the turning point where the market changes its state from bullish to bearish, τ plays the role of the relaxation time of the order of one year, and α is the shape exponent. All the values of parameters and coefficients describing this function for indexes of WIG, DAX, and DJIA bull markets and bear markets are listed in the Tables. A.1–A.12. Notably, the coefficient of determination, R^2, is in no case smaller than $R^2 = 0.9971$. The value of R^2 close to 1 indicates that (A.1) is a properly selected trend. However, such a selection does not exclude the possibility of the existence of a deterministic drift component in the detrended time series. We model the detrended time series entailing this component together with the additive noise in Appendix B. This is done using the first-order difference equation of the stochastic dynamics (B.1), and in particular, locally in the vicinity of a fixed point using Eq. (B.7).

The trend function (A.1) consists of two different components: (i) the main component based on the Mittag-Leffler function monotonically increasing for $t \le t_c$ and monotonically decreasing in the opposite case, and (ii) the higher-order oscillating component (the amplitude X_1 of which is of the order of 10% of the amplitude of the main component $X_0 + X_1$). As required, the trend function obtained in this way mainly exhibits the long-term slowly-varying super-exponential growth, which precedes the speculation-induced crash.

The trend we use is a function that we derived earlier as a rheological model of fractional dynamics of financial markets ([25]). This model introduces the hypothesis that stock markets behave like a viscoelastic biopolymer. That is, they are elastic (i.e., they immediately respond) if the impact of an external force on a stock market is sufficiently strong. But they are more like a liquid (plastic) material in the case of a weak external force. That is, financial markets behave analogically to a non-Newtonian liquid.

Among the fit parameters and coefficients for a given index (see Tables. A.1–A.12), there always exists at least one (characterizing the bull market or bear market) which is burdened by a large standard deviation. In this way the system is protected from arbitrage.

Appendix B. Catastrophic slowing down

In this Appendix, we consider linear indicators of the catastrophic slowing down or regime shift such as: (i) recovery rate and time, (ii) variance, and (iii) reddened power spectra.

Let us suppose that detrended time-dependent time series $x_t \overset{\text{def.}}{=} X(t) - \text{Trend}(t)$, where Trend$(t)$ is the trend expressed by Eq. (A.1), obeys the first-order difference equation of the stochastic dynamics

$$x_{t+1} - x_t = f(x_t; P) + \eta_t = -\frac{\partial U(x_t; P)}{\partial x_t} + \eta_t, \quad \text{(B.1)}$$

where U plays the role of a mechanical potential, the additive noise or stochastic force η_t, $t = 0, 1, 2, \ldots$, is a δ-correlated[9] $(0, \sigma^2)$ random variable. P is a slowly varying

[9] Here, δ is the Kronecker delta, while t indexes trading days within a given trading month (consisting of twenty-one trading days). The trading month is our time window, where λ is approximately constant.

driving (control, in general a vector) parameter, the precise definition of which is given in Appendix C.

In the spirit of the time dependent Ginzburg-Landau theory of phase transition ([50]), we can assume that the potential $U(x; P)$ is a polynomial of the fourth-order (hence, force f is a polynomial of the third-order, cf. Appendix C). Now, our goal is to determine coefficients of this polynomial from the properly detrended empirical data. For instance, in Figs. 7–10 plots of force f, in potential U, and equilibrium probability Pr vs. detrended time series (variable) x are already shown (using solid lines) for different values of parameter P. Furthermore, in the comprehensive Fig. 11, the plots of f are grouped into a three-dimensional visualisation.

Our goal is to utilize potential $U(x; P)$ in the construction of an unconditional equilibrium distribution, $Pr(x; P)$, of the detrended time series and present how both quantities evolve across bistable forms. This will provide a signature of a genuine (and not spurious or artificial) bifurcation transition.

B1. Equilibrium distribution of detrended time series

The differential formulation directly results from Eq. (B.1). Its basic ingredient is the Langevin dynamics [50,55], taking the form of the massless stochastic dynamic equation

$$\frac{\partial x_t}{\partial t} = -\frac{\partial U(x_t; P)}{\partial x_t} + \eta_t. \tag{B.2}$$

This equation is equivalent to the quasilinear (according to van Kampen's terminology, [55]) Fokker-Planck equation

$$\frac{\partial Pr(x, t; P)}{\partial t} = -\frac{\partial j(x, t; P)}{\partial x}, \tag{B.3}$$

which is a form of the continuity equation (a conservation law) for the probability density of the current, i.e. the detrended time series $Pr(x, t; P)$, where the current density is given by the constitutive equation

$$j(x, t; P) = f(x; P)\, Pr(x, t; P) - \frac{\sigma^2}{2}\frac{\partial Pr(x, t; P)}{\partial x}. \tag{B.4}$$

The equilibrium (time-independent) solution of Eq. (B.3) (obtained directly from the requirement that no current is present in the system, (i.e. by assuming that $j(x, t) = 0$ in Eq. (B.4)) is given by

$$Pr(x; P) \sim \frac{2}{\sigma^2}\exp\left(-\frac{2}{\sigma^2}U(x; P)\right), \tag{B.5}$$

where potential $U(x; P)$ already appeared in Eqs. (B.1) and (B.2).

The long-term, slowly-varying evolution of the above given distribution shown in Figs. 7–10 as $U(x; P)$ versus P was found from empirical data (see Appendix C for details). Indeed, the unconditional equilibrium distribution (B.5) exhibits the expected bistable shape slightly before (see Fig. 8) and at the catastrophic bifurcation transition, that is within the bifurcation region (see Fig. 9).

B2. Analysis of the linear stability

In this section, we study the linear stability of the equilibrium, that is we consider the relaxation of the system which was slightly knocked out of equilibrium [56]. The equilibrium of the system is defined by the roots (or fixed points) of the function $f(x; P)$. In Sec. 3, we argue that these roots can be viewed as the mechanical-like equilibria.

The linear expansion of $f(x; P)$ at the fixed point x^*, gives

$$\begin{aligned} y_{t+1} - y_t &= f(x^*(P); P) + \lambda y_t + \eta_t = \lambda y_t + \eta_t \\ &\Leftrightarrow y_{t+1} = AR(1)\, y_t + \eta_t \end{aligned} \tag{B.6}$$

as, by the definition of a root, $f(x^*(P); P)$ vanishes. We will use the following notation: (i) for the displacement from an equilibrium[10] or the (non-normalized) order parameter $y_t = x_t - x^*(P)$, $t = 0, 1, 2, \ldots,$ and (ii) for rate $\lambda(x^*(P); P) = \frac{\partial f(x;P)}{\partial x}\,|_{x=x^*(P)}$. The autoregressive coefficient of the first-order $AR(1) = 1 + \lambda$.

The formula in the second line of Eq. B.6, rewritten in the form

$$x_{t+1} = (1 + \lambda)\, x_t + b + \eta_t,\ b(= A(0)) = -\lambda x^*, \tag{B.7}$$

makes it possible to obtain the recovery rate $-\lambda(> 0)$ and fixed point x^* vs. trading days from the fits to empirical data represented by successive sample regression plots, such as shown, for instance, in Fig. 4.

Each plot in this figure consists of 20 points of daily observations (i.e. covering a single month) at the closing, which appears to be the optimal number for observing the slowing down to zero of the recovery rates shown in the plots in Fig. 5[11] with a satisfactory resolution. The error bar of each individual point placed in these plots comes from the above-mentioned fits as a standard deviation of the straight line slope. (The corresponding points without error bars were found independently from Expression (1)). Obviously, these fits also give the straight line shift b vs. trading days. The resulting combined quantity $-b/\lambda$ is presented in plots in Fig. 6 vs. trading days. We obtain a surprisingly small statistical error for these fits. However, we tacitly assumed that coefficients λ and b were slowly-varying functions of trading days. These fits constitute the empirical basis for our further considerations.

The solution of Eq. (B.6) is

$$\begin{aligned} y_t &= (1 + \lambda)^t y_0 + (1 + \lambda)^{t-1}\sum_{\tau=0}^{t-1}\eta_\tau (1 + \lambda)^{-\tau} \\ &\approx \exp(\lambda t)\left[y_0 + \int_0^t \eta_\tau \exp(-\lambda\tau)d\tau\right] \end{aligned} \tag{B.8}$$

and (as $\langle\eta_\tau\rangle = 0$) its average

$$\langle y_t\rangle = (1 + \lambda)^t y_0 \approx \exp(\lambda t) y_0, \tag{B.9}$$

where the first equality in (B.8) is valid for $t \geq 1$ (for $t = 0$ the solution $y_{t=0} = y_0$). The second approximate equality in (B.8) is valid solely for the case of $|\lambda| \ll 1$ and $t \gg 1$, that is for the immediate vicinity of the threshold (shown in

[10] The set of variables y_t, $t = 0, 1, 2, \ldots,$ is also called the first-order autoregressive time series.

[11] This figure is the result of the linear transformation $(1 + \lambda \Rightarrow -\lambda)$ of Fig. 5. The empirical data points in Fig. 5 are credible, as they come from two independent sources, providing mutually consistent results.

Figs. 2, 3, and 5 by the vertical dashed straight lines) and for a sufficiently long time.

From Eq. (B.9), it follows that a given equilibrium state is stable (i.e., $\langle y_{t\to\infty}\rangle \to 0$ for $y_0 \neq 0$ and $\langle y_t\rangle = 0$ for $y_0 = 0$) if and only if[12] $|1+\lambda| < 1 \Leftrightarrow -2 < \lambda < 0$; otherwise it is unstable. Hence, the local minima of the potential curve (e.g., points 1 and $1''$ in the bottom plot in Fig. 8) define stable equilibria, while the local maximum of the potential curve (e.g., point $1'$ again in the bottom plot in Fig. 8) define the unstable equilibrium. The most relevant states of the system are stable equilibrium points x_1^* and $x_{1''}^*$ shown in Fig. 9 and in Fig. 11 (where they are connected by the arrow), as they define the border of the bifurcation region. Hence, they are referred to as the catastrophic bifurcation points or tipping points. The quantity $\tau \stackrel{\text{def.}}{=} -1/\lambda$ can be interpreted as the relaxation (recovery or return) time solely for the stable (mechanical) equilibria. This is the characteristic time for the system to return to the equilibrium state after being knocked out of it.

B3. Generic properties of the first-order autoregressive time series

It is well-known [7,15] that particularly useful quantities, i.e. variance, covariance and autocorrelation function, as well as the power spectrum, are related. We calculate them by exploiting an exact solution given by the first equality in (B.8).

Firstly, we calculate the covariance,

$$\begin{aligned} Cov(y_t\, y_{t+h}) &= \langle y_t\, y_{t+h}\rangle - \langle y_t\rangle\langle y_{t+h}\rangle = (1+\lambda)^{|h|}\, Var(y_t) = \\ Cov(x_t\, x_{t+h}) &= (1+\lambda)^{|h|}\, Var(x_t) \\ &\Leftrightarrow ACF(h) = \frac{Cov(y_t\, y_{t+h})}{Var(y_t)} \\ &= \frac{Cov(x_t\, x_{t+h})}{Var(x_t)} = (1+\lambda)^{|h|} \\ &\Rightarrow ACF(h) \approx \exp(\lambda\mid h\mid), \\ h &= 0, \pm 1, \pm 2, \ldots, \end{aligned} \tag{B.10}$$

where variance $Var(y_t)$ is given (after straightforward calculations) by the formula

$$\begin{aligned} Var(y_t) &= \left\langle y_t^2\right\rangle - \langle y_t\rangle^2 = Var(x_t) \\ &= Var(y_0)(1+\lambda)^{2t} - \frac{1}{\lambda(2+\lambda)}\left[1-(1+\lambda)^{2t}\right]\sigma^2, \end{aligned} \tag{B.11}$$

where the notation $\langle\ldots\rangle$ denotes an average over the noise and the initial conditions (within the statistical ensemble of solutions y_t given by Eq. (B.8)). The resultant equality in (B.10) is obeyed for $|\lambda| \ll 1$. Furthermore, at a short-time limit, i.e., for $2t \ll N^{-1}$, $Var(y_t)$ simplifies into the form

$$Var(y_t) \approx Var(y_0)(1+2\lambda t) + t\sigma^2 \approx Var(y_0) + \sigma^2 t. \tag{B.12}$$

For the asymptotic time limit, i.e., for $t \to \infty$, Eq. (B.11) reduces (for fixed λ) to the form

$$Var(y_t) \approx -\frac{\sigma^2}{\lambda(2+\lambda)}, \tag{B.13}$$

which diverges for vanishing λ. We hypothesise that by taking into account the flickering phenomenon we will obtain a significant increase in the variance within the bifurcation region. In general, the analytical calculation of variance requires the solution of the nonlinear Eq. (B.1) for f, given, in our case, by the polynomial (defined further in the text by Eq. (C.2)), which remains an unsolved challenge.

The coefficient $1+\lambda$ (present, for instance, in (B.10)) is the lag-1 autocorrelation function, which can be found directly from the empirical data (cf. Fig. 5). Apparently, it does not depend on the variance.

It can be easily proven by using Solution (B.8) that any odd moment of the variable y_t asymptotically vanishes. Hence, from Eq. (B.11), we find that within the linear theory, the skewness also vanishes.

Furthermore, it can be easily verified (by using Solution (B.8)) that the excess kurtosis vanishes if variables y_0 and η_t are drawn from some Gaussian distributions. That is, within the scope of the linear theory (i.e. in the vicinity of the threshold) the distribution of variable y_t can be Gaussian, of variance given by Expression (B.11) and centred around the mean value $\langle y_t\rangle = y_0(1+\lambda)^t$.

Appendix C. Approximation of force *f* by the third-order polynomial

Let us assume that the potential U, used in Eq. (B.1), is defined by the fourth-order polynomial

$$U(x;P) = A_0x^4 + A_1x^3 + A_2x^2 + A_3x + A_4, \tag{C.1}$$

where A_l, $l = 0, 1, \ldots, 4$, are its real coefficients related to the (combined) parameter P – this relation is considered further in this Section. Moreover, we can assume that the coefficient $A_0 > 0$. This is dictated by the empirical data shown in Fig. 6, where the sequence of states (roots) $x_{1''}^*$ and x_1^* placed respectively on the upper and lower segments of the backward folded curves are considered as the stable (mechanical) equilibrium states. Both these roots have opposite signs, which results in the corresponding signs of the coefficients.

According to the definition of potential (see Eq. (B.1)), force f is a polynomial of one order of magnitude lower

$$f(x;P) = a_0x^3 + a_1x^2 + a_2x + a_3, \tag{C.2}$$

here coefficients $a_{4-l} = -l\,A_{4-l}$, $l = 1, \ldots, 4$, where $a_0 < 0$.

Below, we consider following characteristic cases: (a) the catastrophic bifurcation transition at catastrophic bifurcation threshold (regarding Fig. 9), (b) the transition before the catastrophic bifurcation transition (but within bistable region regarding Fig. 8), (c) the transition present after it (regarding Fig. 10) , and (d) the analogous transition present before the bistable region (regarding Fig. 7).

The aim of this Section is to express the coefficients of the polynomial (C.2) in terms of the roots of this polynomial. These roots can be easily extracted from empirical data shown in Fig. 6. Using these coefficients, we are able to plot the force and potential curves (see Figs. 7–10 for details) and give a mechanical interpretation to the catastrophic bifurcation transition.

[12] We observed that for our empirical data a more restrictive inequality $-1 < \lambda < 0$ is obeyed.

C1. Case of the catastrophic bifurcation transition

Let us focus on the case (a) (presented in Fig. 9) concerning the catastrophic bifurcation transition. This means that the coefficients a_l, $l = 0, \ldots, 3$, should provide a corresponding parameterisation, which results in a curve $f(x; P)$ vs. x in the form shown in Fig. 9. (We relate these coefficients to the parameter P at the end of this Section.)

Now, we can provide the detailed goals of this case. They are as follows:

(i) derivation of the root x_1^* and twofold root $x_{1''}^*$ of the polynomial (C.2) and hence calculation, for instance, of the catastrophic bifurcation jump, $\Delta x_{1,1''}^* = x_{1''}^* - x_1^*$, as a function of polynomial coefficients,
(ii) the solution of the inverse problem, that is derivation of the relative parameters a_1/a_0, a_2/a_0, and a_3/a_0 by means of roots x_1^* and $x_{1''}^*$, which can be obtained from the empirical data shown in Fig. 6.

Notably, the catastrophic bifurcation transition $1''\Rightarrow 1$ (cf. the upper plot in Fig. 9 and the transition denoted by the arrow in Fig. 11) beginning at the point $1''$ – which is not only the largest (twofold) root of polynomial f but it also provides the position of its local maximum; hence, it is an inflection point of the curve U vs. x (cf. upper and middle plots in Fig. 9). Considering the canonical representation

$$\frac{1}{a_0} f(x; P) = (x - x_1^*)(x - x_{1''}^*)^2, \tag{C.3}$$

and utilizing Eq. (C.2), we obtain

$$\frac{\partial f(x; P)}{\partial x} \mid_{x=x_0,\, x_{1''}^*} = 0 \Leftrightarrow 3\, x_{0,1''}^{*2} + 2\, \frac{a_1}{a_0}\, x_{0,1''}^* + \frac{a_2}{a_0} = 0,$$
$$\Leftrightarrow x_1^* = \frac{1}{2}(3x_0^* - x_{1''}^*), \tag{C.4}$$

where x_0^* is the first inflection point of the curve U vs. x (see the middle plot in Fig. 9) and it is the local minimum of the curve f vs. x (see the upper plot in Fig. 9). However, this point is not explicitly shown there.

From Eqs. (C.4) and Eq. (C.3), we obtain

$$x_{0,1''}^* = x_{ip}^f \mp \frac{1}{3}\sqrt{D},\ D \stackrel{\text{def.}}{=} \left(\frac{a_1}{a_0}\right)^2 - 3\,\frac{a_2}{a_0},$$
$$x_1^* = x_{ip}^f - \frac{2}{3}\sqrt{D}, \tag{C.5}$$

where for the first upper equation sign $-$ represents the location of the minimum x_0^*, the sign $+$ represents the location of the root $x_{1''}^*$, and we assumed $D > 0$ as both real roots of Eq. (C.4) should exist. Besides, we can easily derive (from the vanishing of the second derivative f over x) that x_{ip}^f, present in (C.5), is the inflection point of f (cf. the upper plot in Fig. 9),

$$\frac{\partial^2 f(x; P)}{\partial x^2} \mid_{x=x_{ip}^f} = 0 \Leftrightarrow x_{ip}^f = -\frac{1}{3}\frac{a_1}{a_0}. \tag{C.6}$$

As follows from Eq. (C.5), both extrema x_0^* and $x_{1''}^*$ are located symmetrically on either sides of the inflection point x_{ip}. That is the position x_0^* of the minimum is located on the left-hand side, while the position of the root $x_{1''}^*$ is on the right-hand side, both being at the same distance from the position of the inflection point.

From Eqs. (C.5), we obtain the catastrophic bifurcation jump in the form of

$$\Delta x_{1,1''}^* = \sqrt{D} = \frac{1}{2a_0}\frac{\partial^2 f(x; P)}{\partial x^2} \mid_{x=x_{1''}^*}, \tag{C.7}$$

which can be easily determined from the curves plotted in Fig. 9. Moreover, the latter equality means that taking into account the quadratic term in the expansion of (B.1) vs. x_t could be a promising approach. A step, based on empirical data, beyond the linear approximation utilized in the derivation of Eq. (B.6), could provide more detailed information, e.g., concerning autocorrelation in the vicinity of the catastrophic bifurcation transition.

From Eqs. (C.5) and (C.6), we derive the solution of the inverse problem in the form,

$$\frac{a_1}{a_0} = -(2x_{1''}^* + x_1^*) \le 0,$$
$$\frac{a_2}{a_0} = x_{1''}^*(x_{1''}^* + 2x_1^*) \ge 0, \tag{C.8}$$

together with the constraint for the relative free parameter

$$\frac{a_3}{a_0} = -x_1^*\,(x_{1''}^*)^2 \ge 0. \tag{C.9}$$

The latter relation makes the above procedure self-consistent.

By identifying the roots $x_1^* = -101.17$ and $x_{1''}^* = 278.92$ from the empirical data shown in Fig. 6(b) as the right tipping point and the one placed on the bifurcation threshold, respectively, we derive the relative parameters in question $a_1/a_0 = -456.67$, $a_2/a_0 = 21359.70$ and $a_3/a_0 = 7.87066 \times 10^6$. Thus, we obtained the unique values of parameters without any fitting routine, i.e. the parameters are not the fitting ones. In addition, the three inequalities given above lead to the following ones: $a_1 \ge 0, a_2 \le 0, a_3 \le 0$. The bottom plots shown in Figs. 8–11 tacitly assume that the parameter P monotonically depends on time (counted on a monthly time scale) at least in the vicinity of the CBT. The vector parameter P consists, in our case, of only two independent components, e.g., x_1^* and $x_{1''}^*$. This is sufficient to perform stochastic simulation at the catastrophic transition point.

C2. Case of the bistable region

The case considered here (i.e., the case represented by Fig. 8) is a generalisation of the one discussed in the subsection above. That is, we consider a variable x placed inside the bifurcation region, where three different real roots exist (cf. backward-folded curves shown in Fig. 6 and schematically shown in Fig. 11).

The goal of this subsection is analogous to that considered above, i.e., to extract coefficients of the polynomial (C.2) by using its roots found from the empirical data (shown in the above mentioned figures). By assuming that the polynomial (C.2) has three real different roots and by comparing Eq. (C.2) with its multiplicative form

$\frac{1}{a_0} f(x;P) = \left(x - x_1^*\right)\left(x - x_{1'}^*\right)\left(x - x_{1''}^*\right)$, we obtain the relations sought for the coefficients of the polynomial

$$\frac{a_1}{a_0} = -(x_{1''}^* + x_{1'}^* + x_1^*),$$
$$\frac{a_2}{a_0} = x_{1'}^* x_{1''}^* + x_1^* x_{1''}^* + x_1^* x_{1'}^*,$$
$$\frac{a_3}{a_0} = -x_1^* x_{1'}^* x_{1''}^*. \quad \text{(C.10)}$$

The equations above are a generalization of the corresponding Eqs. (C.8) and (C.9), as we obtain these by inserting $x_{1'}^* = x_{1''}^*$ in Eqs. (C.10).

Fig. 8 was constructed by using coefficients obtained from Eqs. (C.10) by introducing into their right-hand sides, the following empirical values of the roots: $x_1^* = -626.473$, $x_{1'}^* = -488.308$, $x_{1''}^* = 278.92$, taken, for instance, from the backward-folded curve shown in Fig. 6(b). From (C.10), we obtain the unique values of the relative parameters: $a_1/a_0 = 835.861$, $a_2/a_0 = -5022.94$, $a_3/a_0 = -8.53249 \times 10^8$. Apparently, this situation is analogous to the previous one (considered the above).

C3. Case after the catastrophic bifurcation transition

For this case (represented by Fig. 10), we have an insufficient amount of empirical data for a unique solution, as only a single real root x_1^* can be identified (roots $x_{1'}^*$ and $x_{1''}^*$ are the complex conjugates). Hence, we deal only with a single relation between the coefficients of the polynomial

$$\frac{1}{a_0} f(x_1^*;P) = -(x_1^*)^3 - \frac{a_1}{a_0}(x_1^*)^2 - x_1^* \frac{a_2}{a_0} - \frac{a_3}{a_0} = 0, \quad \text{(C.11)}$$

which makes the ratio of the parameters a_3/a_0 dependent on x_1^*, a_1/a_0, and a_2/a_0. Therefore, the driving vector parameter can be defined as $P = (x_1^*, a_1/a_0, a_2/a_0)$, where relative parameters a_1/a_0 and a_2/a_0 are free. For instance, in Fig. 10 we show plots for the root $x_1^* = -75.3875$, as well as the ratios of the parameters $a_1/a_0 = -456.67$, $a_2/a_0 = 41709.50$, and $a_3/a_0 = 6.1682 \times 10^6$.

C4. Case before the bistable region

We deal with an analogous situation as given above if x is placed before the catastrophic bifurcation region and (simultaneously) outside of the bistable region. Then, we are again dealing with a single real root, e.g., $x_{1''}^* = 421.009$, while the roots x_1 and $x_{1'}^*$ are complex conjugates. For instance, in Fig. 7 we show plots for the ratios of the parameters $a_1/a_0 = 1179.81$, $a_2/a_0 = 278390$ and $a_3/a_0 = -4.00948 \times 10^8$.

Fortunately, the cases represented by Figs. 7 and 10, and defined by two free relative parameters a_1/a_0 and a_2/a_0, are not particularly interesting because the regions concerned are outside the most interesting bistable regime.

References

[1] Albert R, Barabási A-L. Statistical mechanics of complex networks. Rev Mod Phys 2001;74:47–97.
[2] . In: Albeverio S, Jentsch V, Kantz H, editors. Extreme events in nature and society. Berlin: Springer-Verlag; 2006.
[3] Badii R, Politi A. Complexity. Hierarchical structures and scaling in physics. Cambridge: Cambridge Univ. Press; 1997.
[4] Barunik J, Vosvrda M. Can a stochastic cusp catastrophe model explain stock market crashes? J Econ Dyn Control 2009;33:1824–36.
[5] Bełej M, Kulesza S. Real estate market under catastrophic change. Acta Phys Pol 2013;123:497–501.
[6] Brock WA, Carpenter SR, Scheffer M. Regime shifts, environmental signals, uncertainty and policy choice. In: Norberg J, Cumming G, editors. A theoretical framework for analyzing social-ecological systems. New York: Columbia Univ. Press; 2006. p. 180–206.
[7] Brockwell PJ, Davis RA. Time series: theory and methods,. Berlin: Springer-Verlag; 1991.
[8] Carpenter SR, Brock WA. Rising variance: a leading indicator of ecological transitions. Ecol Lett 2006;9:308–15.
[9] Carpenter SR, Brock WA, Cole JJ, Kitchell JF, Pace ML. Leading indicators of trophic cascaders. Ecol Lett 2008;11:128–38.
[10] Chang G, Feigenbaum J. A bayesian analysis of log-periodic precursors to financial crashes. Quant Finance 2006;6:15–36.
[11] Dorogovtsev SN, Goltsev AV, Mendes JFF. Critical phenomena in complex networks. Rev Mod Phys 2008;80:1275–335.
[12] Fantazzini D, Geraskin P. Everything you always wanted to know about log-periodic power laws for bubble modelling but were afraid to ask. Eur J Finance 2013;19:366–91.
[13] Filimonov V, Sornette D. Spurious trend switching phenomena in financial markets. Eur Phys J B 2012;85(155/1-5).
[14] Fry JM. Exogenous and endogenous market crashes as phase transitions in complex financial systems. EPJ B 85 2012;405.
[15] Fuller WA. Introduction to statistical time series. Canada: J. Wiley & Sons, Inc.; 1976.
[16] Gottinger H-W. Complexity and catastrophe, applications of dynamic system theory. In: Kýn O, Schrettl W, editors. On the stability of contemporary economic systems: proceedings of the third Reisenburg Symposium. Göttingen: Vandenhoeck & Ruprecht; 1979. p. 422–38.
[17] Guttal V, Jayaprakash C. Changing skewness: an early warning signal of regime shifts in ecosystems. Ecol Lett 2008;11:450–60.
[18] Haldane AG, May RM. Systemic risk in banking ecosystems. Nature 2011;469:351–5.
[19] Hohenberg P, Halperin B. Theory of dynamic critical phenomena. Rev Mod Phys 1977;59:435–79.
[20] Jakimowicz A. Catastrophes and chaos in business cycle theory. Acta Phys Pol A 2010;117:640–6.
[21] Jiang SM, Cai SM, Shou T, Zhou PL. Note on two-phase phenomena in financial markets. Chin Phys Lett 2008;25(6):2319–22.
[22] Johnson N. Proposing policy by analogy is risky. Nature 2011;469.302–302
[23] Johnson NF, Hui PJ. Financial market complexity. Oxford: Oxford Univ. Press; 2007.
[24] Paul W, Baschnagel J. Stochastic processes. From physics to finance. Berlin: Springer-Verlag; 1999.
[25] Kozłowska M, Kasprzak A, Kutner R. Fractional market model and its verification on the warsaw stock exchange. Int J Mod Phys C 2008;19:453–69.
[26] Kozłowska M, Kutner R. Singular dynamics of various macroeconomic sectors. Acta Phys Pol 2010;117:630–6.
[27] Kutner R, Binder K, Kehr KW. Diffusion in concentrated lattice gases. v. particles with repulsive nearest-neighbor interaction on the face–centered-cubic lattice. Phys Rev B 1983;28:1846–58.
[28] Landau DP, Binder K. A guide to Monte Carlo simulations in statistical physics. Cambridge: Cambridge Univ. Press; 2000.
[29] Lux T. Network theory is sorely required. Nature 2011;469.303–303
[30] Malevergne Y, Sornette D. Extreme financial risks. From dependence to risk management. Berlin: Springer-Verlag; 2006.
[31] Mandelbrot B, Wallis J. Computer experiments with fractional gaussian noises. Water Resour Res 1969;5:228–67.
[32] Mantegna RN, Stanley HE. An Introduction to econophysics. Correlations and complexity in finance. Cambridge: Cambridge Univ. Press; 2000.
[33] Matia K, Yamasaki K. Statistical properties of demand fluctuation in the financial market,. Quant Finance 2005;5(6):513–17.
[34] McSharry PE, Smith LA, Tarassenko L, Martinerie J, Quyen MLV, Baulc M, et al. Prediction of epileptic seizures: are nonlinear methods relevant? Nat Med, Lett Editor 2003;9(3):241–2.
[35] Metzler R, Klafter J. The random walk's guide to anomalous diffusion: a fractional dynamics approach,. Phys Rep 2000;339:1–77.
[36] Plerou V, Gopikrishnan P, Stanley HE. Two phase behaviour of financial markets. Nature 2003;421:129–30.
[37] Plerou V, Gopikrishnan P, Stanley HE. Two phase behaviour and the distribution of volume. Quant Finance 2005;5:519–21.

[38] Potters M., Bouchaud J.-P.. Comment on "two-phase behavior of financial markets. 2003. ArXiv.cond-mat/0304514v1.
[39] Preis T. Econophysics: complex correlations and trend switchings in financial time series. Eur Phys J ST 2011;194(1):5–86.
[40] Preis T, Schneider JJ, Stanley HE. Switching phenomena in financial markets. PNAS 2011;108(19):7674–8.
[41] Preis T, Stanley HE. Switching phenomena in a system with no switches. J Stat Phys 2010;138(1-3):431–46.
[42] Preis T, Stanley HE. Trend switching processes in financial markets. In: Takayasu M, Watanabe T, Takayasu H, editors. Econophysics approaches to large-scale business data and financial crisis. Tokyo: Springer-Verlag; 2010. p. 3–26.
[43] Preis T, Stanley HE. Bubble trouble. Phys World 2011;24:29–32.
[44] Preis T, Stanley HE. How to characterize trend switching processes in financial markets. Bull Asia Pacific Cent Theor Phys 2009;23:18–23.2009
[45] Roehner BM. Patterns of speculation. A Study observational econophysics. Cambridge: Cambridge Univ. Press; 2002.
[46] Rosser JB Jr. Implications for teaching macroeconomics of complex dynamics. Dept. Economics, James Madison Univ., Harrisonburg; 2004.
[47] Schadschneider A, Chowdhury D, Nishinari K. Stochastic transport in complex systems. From molecules to vehicles. Amsterdam: Elsevier; 2011.
[48] Scheffer M, Bascompte J, Brock WA, Brovkin V, Carpenter SR, Dakos V, et al. Early-warning signals for critical transitions. Nature 2009;461:53–9.
[49] Sornette D. Why stock markets crash. Princeton and Oxford: Princeton Univ. Press; 2003.
[50] Sornette D. Critical Phenomena in Natural Sciences. Chaos, fractals, selforganization and disorder: concepts and tools. Springer series in synergetics. 2nd ed. Heidelberg: Springer-Verlag; 2004.
[51] Nawrocki D, Vaga T. A bifurcation model of market returns. Quant Finance 2014;14(3):509–28.
[52] Sornette D. Dragon-kings, black swans and the prediction of crises. Int J Terraspace Eng 2009;2:1–17.
[53] Stanley HE, Buldyrev SV, Franzese G, Havlin S, Mallamace F, Kumar P, et al. Correlated randomness and switching phenomena. Physica A 2010;389:2880–93.
[54] Vandewalle N, Ausloos M, Boveroux P, Minguet A. Visualizing the log-periodic pattern before crashes,. Eur J Phys B 1999;9:355–9.
[55] van Kampen NG. Stochastic processes in physics and chemistry. Amsterdam: North-Holland; 1987.
[56] Wissel C. A universal law of the characteristic return time near thresholds, 65. Berlin: Oecologia; 1984. p. 101–7.
[57] Zeeman EC. On the unstable behavior of stock exchanges. J Math Econ 1 1974:39–49.
[58] Zeeman EC. Catastrophe theory: selected papers, 1972-77. Bull Amer Math Soc (N S) 1978;84:1360–8.Errata, Bull. Amer. Math. Soc. (N. S.) 1, 681–681 (1979)
[59] Zeeman EC. Evolution of catastrophe theory. Understanding catastrophe,. Cambridge: Cambridge Univ. Press; 1992.
[60] Zheng B, Qiu T, Ren F. Two-phase phenomena, minority games, and herding. Phys Rev E 2004;69(046115/1-6).